

1 **Liquid Structure and Dynamics in Acetaline, a Choline Acetate:Urea 1:2 Deep Eutectic Solvent.**

2
3
4 Alessandro Triolo^{1,*}, Maria Enrica Di Pietro², Andrea Mele², Fabrizio Lo Celso^{1,3}, Martin Brehm⁴,
5 Valerio Di Lisio⁵, Andrea Martinelli⁵, Philip Chater⁶, and Olga Russina^{1,5,*}.

6
7 ¹ Laboratorio Liquidi Ionici, Istituto Struttura della Materia, Consiglio Nazionale delle Ricerche, (ISM-
8 CNR) Rome, Italy

9 ² Department of Chemistry, Materials and Chemical Engineering “G. Natta”, Politecnico di
10 Milano, Milano, Italy.

11 ³ Department of Physics and Chemistry, Università di Palermo, Palermo, Italy.

12 ⁴ Institut für Chemie, Martin-Luther-Universität Halle–Wittenberg, Halle (Saale), Germany.

13 ⁵ Department of Chemistry, University of Rome Sapienza, Rome, Italy.

14 ⁶ Diamond House, Harwell Science & Innovation Campus, Diamond Light Source, Ltd.,
15 Didcot, Oxfordshire OX11 0DE, UK

16
17
18
19 Corresponding Authors: A. T. (triolo@ism.cnr.it); O.R. (olga.russina@uniroma1.it)

21 **Abstract.**

22 We report on the thermodynamic, structural and dynamic properties of a recently proposed Deep
23 Eutectic Solvent (DES), formed by choline acetate and urea at the stoichiometric ratio 1:2, hereinafter
24 indicated as acetaline. Acetaline, although melting at ca. 40 °C, can be easily supercooled in its liquid
25 state at sub-ambient conditions. The existence of a crystalline phase has been detected, together with
26 the glass-liquid transition at -50 °C. Synchrotron high energy X-ray scattering experiments provide the
27 experimental data for supporting a Reverse Monte Carlo analysis to extract structural information at
28 atomistic level. This exploration of acetaline's liquid structure reveals the major role played by
29 hydrogen bonding in determining interspecies correlations: both acetate and urea are strong hydrogen
30 bond acceptor sites, while both the choline hydroxyl and urea act as HB donors. All acetaline moieties
31 are involved in mutual interactions, with acetate and urea strongly interacting through hydrogen
32 bonding, while choline being involved mostly in van der Waals mediated interactions. Such a structural
33 situation is mirrored by the dynamic evidences obtained by means of ¹H NMR techniques, that show
34 how urea and acetate species experience higher translational activation energy than choline,
35 fingerprinting their stronger commitments into the extended hydrogen bonding network established in
36 acetaline.

37

38

39

40

41

42

43

44 **Introduction.**

45

46 In the last decade large interest has been growing around deep eutectic solvents (DES)^{1,2} and their
47 applications in several fields³⁻⁸. After the classification proposed by Smith et al. of DES in terms of
48 four different types³, those belonging to type III are among the most commonly encountered ones.
49 These latter DES are composed by a mixture of a salt (e.g. choline (i.e. the (2-hydroxyethyl)-
50 trimethylammonium cation) chloride) with a hydrogen bonding donor (such as urea, glycerol, etc.)
51 with, depending on the concentration ratio between the two components, a melting point depression
52 resulting from their mixing. The large interest on these compounds stems from several appealing
53 properties, not least their cheap production cost and easy preparation and purification. Most of them are
54 also characterised by nonflammability, bio-compatibility and low toxicity, thus turning out to be ideal
55 media for the development of a variety of processes. On the other hand, most of these appealing
56 features stem from the combination of chemical-physical properties of the different components.
57 Accordingly, by (even minor) changes to their chemical nature, one can efficiently modulate the
58 resulting macroscopic performance, thus leading to the classification of DES as task-specific solvents.⁴
59 Among the most well-known DES, we recall the stoichiometric 1:2 mixture of choline chloride (CC)
60 and urea (U), sometimes referred to as reline.⁹⁻¹⁶ Dry reline melts at ca. 31 °C¹⁷ and has attracted huge
61 interest over the last few years. Other CC-based DES have been proposed, including CC-glycerol (Gly)
62 1:2 (glyceline)¹⁸⁻²², CC-ethylen glycole (EG) 1:2 (ethaline)²²⁻²⁴ and, more recently, CC-water 1:3.3-4.2
63 (aquoline)²⁵⁻²⁷. The recent interest in DES stems from the opportunity that they provide to modulate
64 their solvating properties by changes in their chemical composition. Aiming at expanding the spectrum
65 of properties, other anions paired with choline have been explored as well. For example, choline acetate
66 (Cac) has been recently considered as an interesting ionic liquid to be paired with an HB donor to lead
67 to a DES. Cac is an ionic liquid with melting point at 51 °C, proposed by Fukaya et al., as an
68 interesting example of an IL composed solely of biomaterials.²⁸ The opportunity to use it as a salt for
69 preparation of a DES was presented by Zhao et al., who showed the eutectic nature of mixtures of Cac
70 with urea (1:2), Gly and EG; these DES showed low viscosity, high biodegradability and excellent
71 compatibility with lipase.²⁹ More recently Cac mixtures with different HBDs were probed for their
72 efficiency towards enzymatic reaction with β -galactosidase.³⁰ In 2020, some of us used Cac-based
73 DES in order to efficiently solubilise hemicellulose at mild conditions.³¹

74 This intense applicative activity calls for deeper understanding of the chemical-physical properties of
75 CAc-based DES that have so far received negligible attention compared e.g. to their CC-based
76 equivalents. Here we present a detailed experimental and computational study of structural and
77 dynamic properties of liquid acetaline, a DES composed by CAc and urea at 1:2 molar ratio. The
78 structural properties of acetaline have been obtained by merging high-energy X-ray diffraction and a
79 Reverse Monte Carlo computational approach, aiming at extracting atomistic level structural details of
80 the liquid organization in bulk acetaline. The same sample has also been probed with NMR techniques,
81 aiming at extracting dynamic information related to rotational and translational processes, occurring
82 around room temperature. Overall, this study provides a careful characterization of structural and
83 dynamic properties of a new, eco-sustainable DES, paving the way for its application as a
84 complementary medium to other related DES.

85

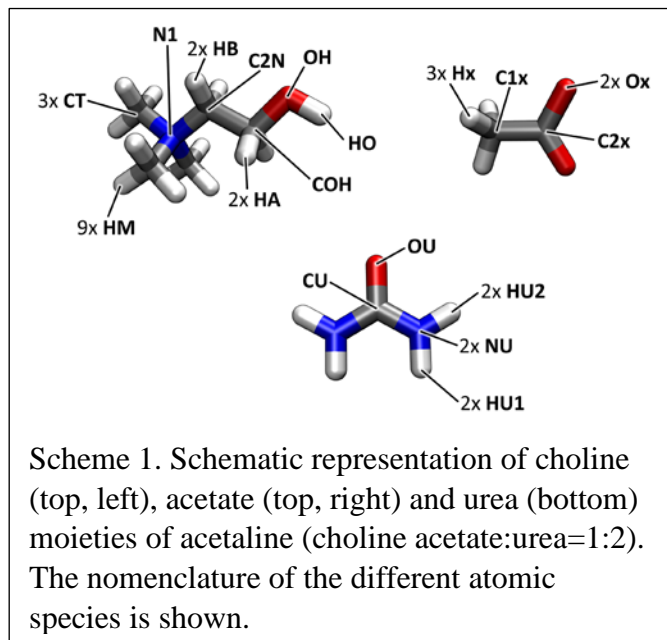
86

87

88

89 **Experimental and Computational details.**

90 Choline acetate (CAc) used for DSC and X-ray scattering was a TCI product; urea was a Sigma
91 Aldrich product. CAc and urea were dried under vacuum at ambient temperature for several days.
92 Eutectic mixtures at 1:2 CAc:U ratio were prepared in a glovebox with an inert atmosphere to reduce
93 ambient moisture contamination, leading to acetaline formation (see **Scheme 1**). After mixing, the
94 sealed vials were kept at 40 °C under constant agitation for at least one hour, to lead to a transparent



106

homogeneous liquid. The sample could be maintained amorphous, when kept at ambient temperature (20 °C) in thin sealed capillaries; it would crystallise when kept inside large sealed vials.

DSC thermograms were acquired by a Mettler Toledo DSC 822e equipped with a FRS5 sensor and a liquid nitrogen cooler. The furnace was purged during the measurement with dry nitrogen at a flow rate of 30 ml min⁻¹. A sample of about 5 mg was weighted in a 40 µl aluminium pan and rapidly sealed. DSC scans comprised of a cooling

107 from 50 to -125 °C followed by a heating from -125 °C up to 50 °C, with a heating/cooling rate of 2/10
108 °C min⁻¹.

109 Acetaline was loaded into a borosilicate capillary of 1.5 mm outer diameter, which was glue-sealed.
110 The total high-resolution X-ray scattering data were collected on the I15-1 beamline at Diamond Light
111 Source, UK, using X-rays of wavelength 0.309574 Å and a Perkin Elmer XRD 4343 CT detector. The
112 total scattering data were integrated to 1D using DAWN³² and then normalised and corrected to extract
113 S(Q) using GudrunX^{33,34}.

114 CAc and U for NMR experiments were purchased from Iolitec and Sigma Aldrich, respectively, and
115 used without further purification. The DES at 1:2 molar ratio was prepared by the heating method, by
116 mixing the two constituents at 80 °C under stirring for 1h, until a homogeneous and transparent liquid
117 was formed. As the freshly prepared acetaline nor its starting components were dried, a residual
118 amount of water is present in the sample (5.7 wt% by Karl Fischer titration). **Controlled amounts of**

119 water are beneficial to reduce the viscosity and allow for satisfactorily resolved NMR spectra. The
120 sample was transferred to a 5 mm NMR tube, equipped with a capillary containing DMSO-d₆. NMR
121 measurements were performed at 11.74 T NMR with a Bruker NEO 500 console equipped with a direct
122 observe BBFO (broadband including fluorine) iProbe (¹H resonance frequency of 500.13 MHz).
123 Measurements were performed over a temperature range of 278 K to 358 K, in 5 K increments, and a
124 minimum of 15 min allowed for thermal equilibration. The residual amount of water together with the
125 liquid tendency to remain in a supercooled state when slowly cooled (see Results & discussion)
126 allowed for NMR measurements at such temperatures.

127 T₁ relaxation measurements were carried out without sample spinning with the inversion recovery (IR)
128 pulse sequence, using relaxation delays at least five times the longest T₁, and the instrument was
129 carefully tuned, shimmed, and the 90° pulses calibrated before each measurement. The spin–lattice
130 relaxation rates were measured using data matrices of 16384 (t₂) × 16 (t₁), over a spectral width of 9
131 ppm for various delay times τ, ranging from 0.05–5 to 0.05–12 s, according to the temperature. A total
132 of two transients per increment were collected for each T₁ experiment. The baselines of all arrayed T₁
133 spectra were corrected prior to processing the data and integrals were used to calculate relaxation times.
134 A single exponential decay was observed for all samples over the entire temperature range investigated.
135 Relaxation times were computed from experimental raw data by means of the Bruker T₁/T₂ relaxation
136 module using the manual integration option and applying the standard one-component fitting function.
137 Data were processed three times and errors were calculated from the maximum standard deviation
138 found at the lowest temperature. Maximum errors are estimated to be 1%. Fits to extract the correlation
139 times and rotational activation energies from the relaxation rates were performed with OriginPro 2018
140 using a user-defined function with the Levenberg–Marquardt algorithm. For the fit procedure, average
141 errors were estimated to be 5%

142 Self-diffusion coefficients were measured by pulsed field gradient (PFG) experiments by applying sine-
143 shaped pulsed magnetic field gradients along the z-direction up to a maximum strength of G = 53.5 G
144 cm⁻¹. All the diffusion experiments were performed using the bipolar pulse longitudinal eddy current
145 delay (BPP-LED) pulse sequence. All experiments were carried out over a spectral width of 9 ppm,
146 with a total of eight transients per increment. The relaxation delay was set to at least five times T₁, and
147 four dummy scans were programmed prior to acquisition. The pulse gradients were incremented from 2
148 to 95% of the maximum gradient strength in a linear ramp with 32 steps. For each DOSY experiment,

149 the duration of the magnetic field pulse gradients (δ) and the diffusion times (Δ) were optimized to
150 obtain, where possible, 95% signal attenuation for the slowest diffusion species at the last step
151 experiment. δ values were in the 2.4–6 ms range, while Δ values were 0.4–0.8 s long. The baselines of
152 all arrayed spectra were corrected prior to processing the data. Data were processed using an
153 exponential filter in F2 dimension (LB = 0.3 Hz), and integrals were used in calculating relaxation
154 times. The determination of self-diffusion coefficients used the Bruker T₁/T₂ module of TopSpin for
155 each peak. The precision of the measured diffusion coefficients is estimated to be within 3%.

156 2D ¹H-¹H nuclear Overhauser enhancement (NOESY) experiments were recorded at 298 K by using
157 the phase-sensitive ge-2D NOESY pulse sequence using echo-antiecho (noesyetgp in the Bruker
158 library). Spectra were recorded using eight transients over 4096 (t₂) × 256 (t₁) complex data points. 32
159 dummy scans and mixing times in the range 20 – 500 ms were used. The relaxation delay was set to 4
160 s. The NOESY data sets were processed by applying a sine squared window function in both
161 dimensions (SSB = 2) prior to the Fourier transform.

162 The EPSR approach has been used to model the X-ray diffraction data.³⁵ This is a robust approach
163 that is based on the optimization of the empirically proposed potential that leads to the best agreement
164 with experimental diffraction data.

165 We used a simulation box containing 100 CAc ion pairs and 200 urea moieties (CAc:Urea=1:2) with
166 a density of 1.17 g/cc³⁰ (cubic box size=35.3 Å) at 25 °C. The starting interatomic potential used for
167 choline and urea is the one that was successfully used by Hammond et al. in their study of reline.^{10,36}
168 The acetate interaction potential parameters are the same used by Bowron et al. in their study of acetate
169 based ionic liquids.³⁷ After an equilibration of ca. 6,000 steps, the EPSR was activated and further
170 10,000 steps delivered a good agreement of the calculated diffraction pattern with the experimental
171 one. At this stage, further 7,000 steps were collected to achieve statistical accuracy on the structural
172 observables (pair distribution functions, angular distributions etc.). In order to evaluate structural
173 properties from the resulting Monte Carlo trajectories, the TRAVIS software was used.^{38–40}

174

175

176 **Results & discussion.**

177 Acetaline's DSC trace is shown in **Figure 1**, where two thermal traces are shown with heating/cooling
178 rates equal to 2 and 10 °C/min, respectively. At ambient conditions (i.e. at ca. 20 °C), crystalline
179 acetaline is thermodynamically stable, with a melting temperature of about 40 °C. It appears that upon
180 cooling, liquid acetaline can be easily supercooled into an amorphous solid, without crystallization
181 intervening. The liquid-glass transition can be detected at approximately -50 °C. On the other hand,
182 upon heating the glass material, crystallization occurs at temperatures depending on the heating rate;
183 such a crystal eventually melts approaching 36-38 °C.

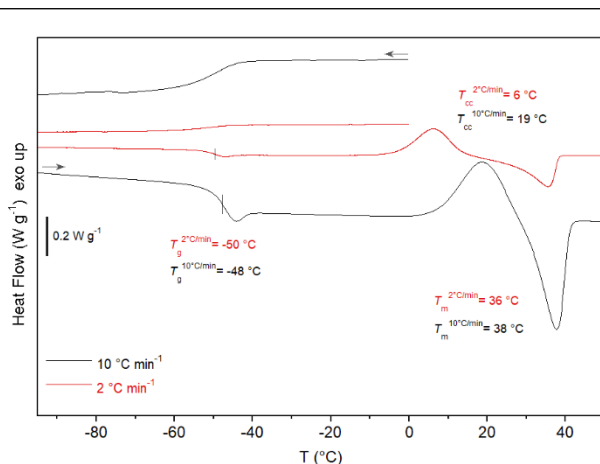


Figure 1. Thermal trace of acetaline (choline acetate: urea=1:2) at two different heating/cooling rates (2 and 10 °C/m, respectively). Indications of the liquid-glass transition at ca. -50 °C and solid melting at ca. 38 °C are highlighted.

184 It is noteworthy that, upon cooling from the melt, acetaline remains in the liquid supercooled state at
185 20 °C for long time (several days). Accordingly, we determined the liquid structure of acetaline at
186 ambient temperature, without incurring into sample crystallization during the experiment time duration.
187 Synchrotron X-ray diffraction data collected in such a way are reported in **Figure 2**. It appears that
188 acetaline is characterised by an X-ray diffraction pattern similar to the ones from other choline-based
189 DES, such as reline, aquoline etc.

190 The quality of the agreement of experimental X-ray scattering pattern and the corresponding EPSR
191 computed quantity is shown in **Figure 2**. The EPSR-derived X-ray weighted scattering pattern nicely
192 accounts for the experimentally observed features, thus providing a validation support to the structural
193 information that can be extracted from the computed trajectories. It can be appreciated that similarly to
194 other choline-based DES, the experimental X-ray scattering pattern does not show appreciable features

195 at low Q values, apart from the low Q peak at ca. 1.5 \AA^{-1} , thus suggesting that no large scale structural
196 heterogeneities occur in this system, which could be related either to polar/apolar segregation⁴¹⁻⁴⁴ or to

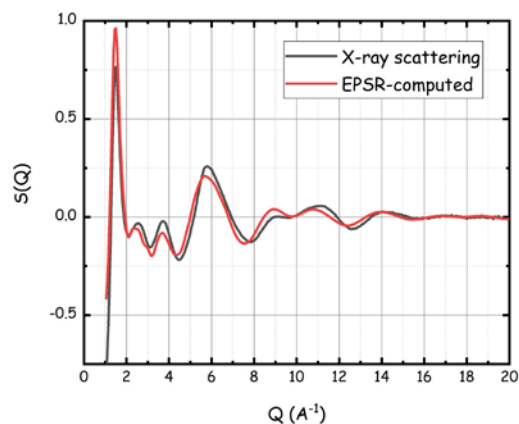


Figure 2. Comparison between experimental (black) and EPSR-computed (red) X-ray scattering patterns from acetaline at ambient temperature.

197 mesoscopic phase separation⁴⁵⁻⁴⁷. The EPSR-generated trajectories were further interrogated to extract
198 structural information on bulk acetaline.

199 **Figures 3** shows the center of mass pair distributions functions (pdf) for the three moieties in acetaline,
200 namely, choline cation (C), acetate anion (A) and urea (U). It emerges that strong correlations exist
201 between differently charged ionic species and between urea and all the components. Correlations
202 between ionic species with the same charge are instead weaker and less well defined. CC correlations

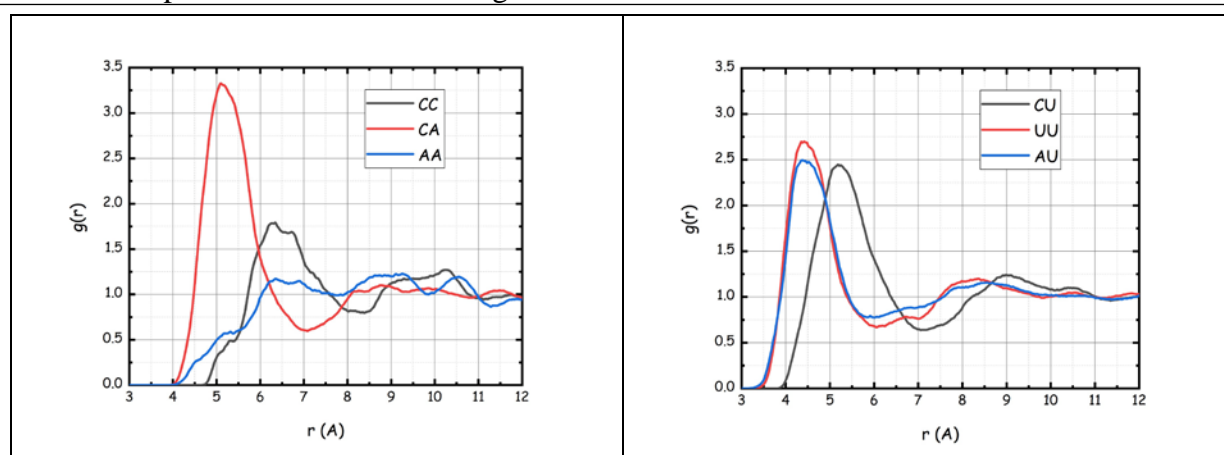


Figure 3. Pair distribution function between centers of mass of ionic species (cation (C), anion (A)) (left) and urea (U) with A and C (right) in acetaline, as obtained from the EPSR modelling.

203 are characterised by a weak broad peak centred at ca. 6.5 Å, building up a solvation shell containing ca.
 204 3 moieties. This coordination number is substantially different from what is found in the case of reline,
 205 where choline is surrounded by approx. 6 other choline cations. Such a situation likely stems from the
 206 larger size, as well as the different shape and symmetry of acetate as compared to chloride anions. Each
 207 choline cation is on average surrounded by 3.4 acetate anions with a correlation peak at 5.3 Å. For
 208 comparison in reline, 4.5 chloride anions were found in the first shell¹⁰, while 1 chloride anion was
 209 found in the same shell in malicine⁴⁸. Urea is characterised by strong correlations both with other urea
 210 moieties and with both cations and anions. First solvation shells are detected around each ionic species,
 211 with peaks centred at 5.1 Å and 4.5 Å and 6 and 4 nearest neighbour urea moieties for choline and
 212 acetate, respectively.

213 **Figure 4** reports a series of pdfs related to selected correlations between atomic species belonging to
 214 the different moieties building up bulk acetaline.

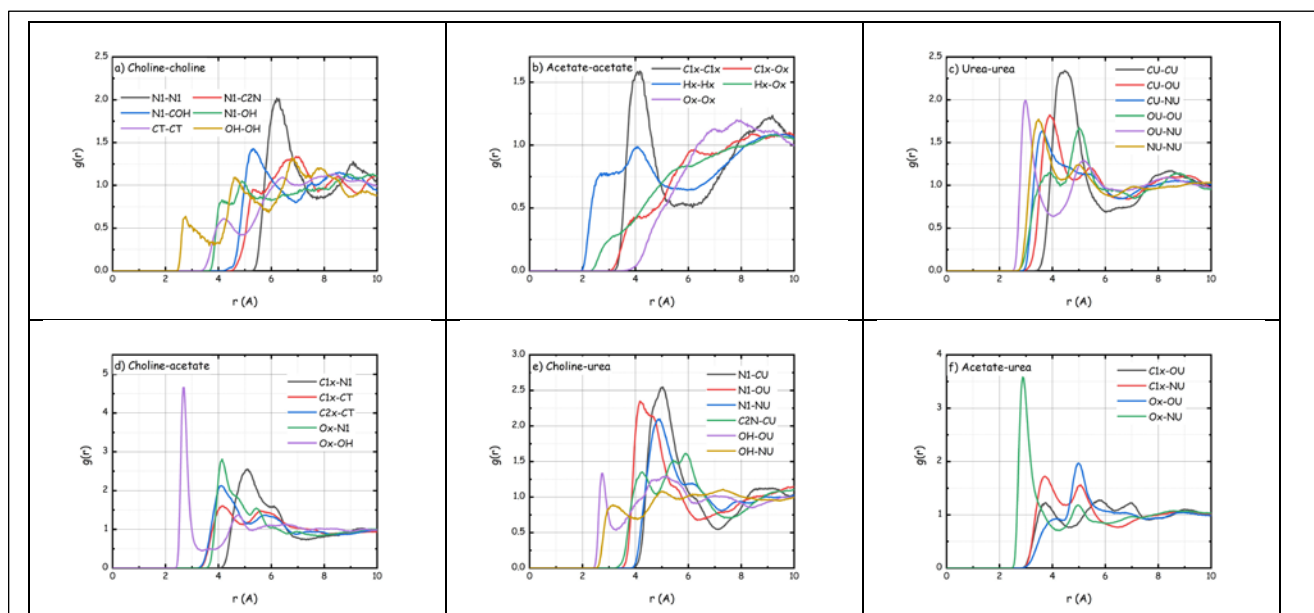


Figure 4. Selected pair distribution functions between different atomic species belonging to the three moieties in acetaline (choline, acetate and urea, respectively), after the EPSR modelling.

215 The selected pdfs indicate the existence of strong correlations between the different moieties. In
 216 particular, those pdfs involving acetate and either choline or urea, are characterised by strong peaks,
 217 fingerprinting hydrogen-bonding mediated interactions. Such interactions will be further explored later
 218 in the manuscript. Choline-choline correlations are rather weak and broadly distributed. The strongest
 219 correlation is between neighbour nitrogen atoms, with a peak centred at 6.5 Å, and a neighbour number

220 of ca. 2.5 up to 7 Å. We also detect a relatively strong N1-COH correlation centred at ca. 5.3 Å with
221 approximately 2.5 nearest neighbours (n.n.); however there is only weak interaction of the nitrogen
222 with the hydroxyl group (weak peaks for N1-OH between 4 and 5 Å). Neighbour acetate anions are
223 only correlated through their methyl groups for which we detect a C1x-C1x peak at 4 Å, with one
224 methyl group directly correlated to the reference one. Urea-urea correlations look more structured: we
225 will see later that this is also because of the existence of hydrogen bonding interactions and accordingly
226 we find strong peak in the OU-NU pdf at ca. 3 Å, with a n.n. population of 2 NUs around the reference
227 OU. The other peaks reported in **Figure 4 c)** indicate the existence of strong correlations also between
228 other urea's moieties such as NU-NU (3 n.n.), CU-OU (2 n.n.) and, in particular, CU-CU (4 n.n.).
229 Similar observations led Edler et al. to propose the existence of urea clustering in reline.¹⁰ Inter-species
230 correlations are dominated, as we will see later in more detail, by HB correlations. Overall these
231 correlations look much stronger than correlations between similar species. The selected pdfs in **Figures**
232 **4 d)-f)** reflect in an indirect way the existence of such interactions. Choline-acetate correlations are
233 characterised by a strong Ox-OH peak at 2.7 Å, fingerprinting the HB between the two species. The
234 broad peak related to the Cation-Anion pdf in **Figure 3** is likely related to the existence of different
235 solvation scenarios of acetate around the reference choline: in particular, acetate will coordinate choline
236 both at the hydroxyl side and at the ammonium side. This latter scenario is fingerprinted in the Ox-N1
237 and C1x-N1 pdfs by the strong peaks centred at 4.2 and 5 Å, respectively. Choline and urea appear to
238 interact mostly through choline's ammonium: pdf peaks for N1 with CU, NU and OU are eminent at
239 distances between 4 and 5.5 Å. Correlations mediated through choline's hydroxyl group look weaker.
240 The competition between acetate and urea in coordinating choline's N1 leads to ca. 5 urea and 3 acetate
241 moieties surrounding N1 by a distance of ca. 7 Å. For comparison, the OH moiety of choline is
242 solvated by 0.6 acetate and 0.9 urea in the first shell (up to 4.5 Å) and ca. 2 choline in the first shell (up
243 to 7 Å). Acetate and urea interact through HB involving urea's hydrogen and the carboxyl group; such
244 an interaction, fingerprinted by the Ox-NU peak at ca 3 Å, is consistent with two different solvation
245 environments indicated by the two peaks in the C1x-NU pdf (3.7 and 5 Å).

246 As mentioned, HB interactions are fundamental in driving structural correlations in acetamine. In **Figure**
247 **5**, the pair distribution functions associated to such correlations involving either the choline HOH or the
248 urea HU1/2 donor groups. In particular, we specifically monitor the two hydrogens, HU1 and HU2,
249 attached to the same nitrogen in urea (HU1 being the hydrogens in trans with the urea's oxygen and
250 HU2 being the cis hydrogens), aiming at assessing differences in the HB features, due to steric

251 hindrance. In all cases, HB involving the acetate HB acceptor (Ox) are characterised by the shortest and

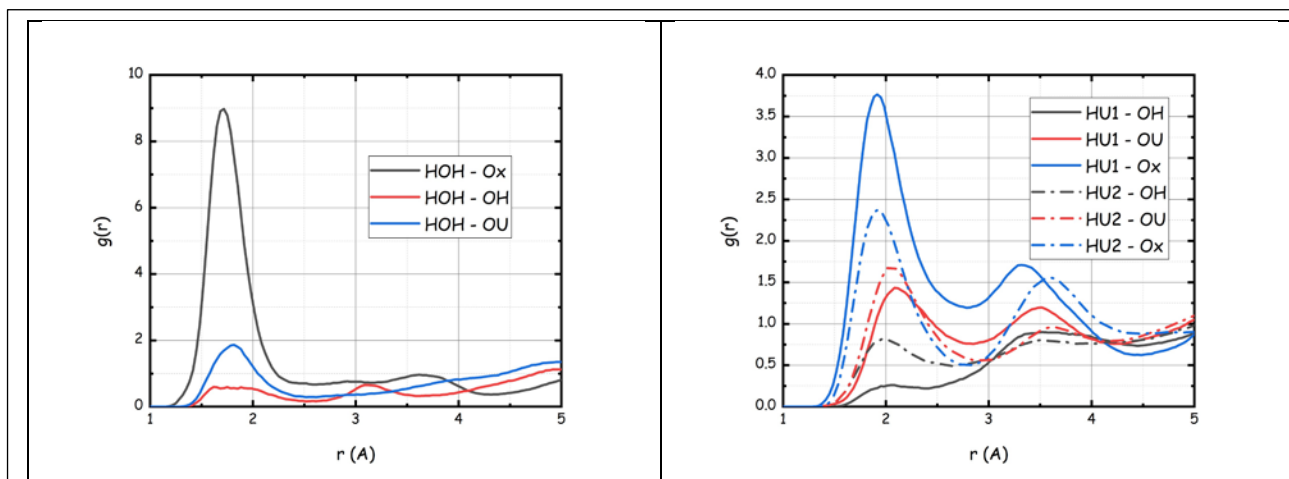


Figure 5. Pair distribution functions related to hydrogen bonding interactions in acetaline, as obtained from the EPSR modelling: (left) pdf related to the HOH donor agent in choline and (right) pdf related to the trans (HU1) and cis (HU2) hydrogens in urea.

252 strongest interaction. In terms of pdf peak amplitude, the next most intense peaks correspond to those
 253 involving urea's oxygen (OU) and finally choline's oxygen (OH). In order to better illustrate the
 254 balance between HB donor and acceptor capabilities of the different moieties in acetaline, we exploit

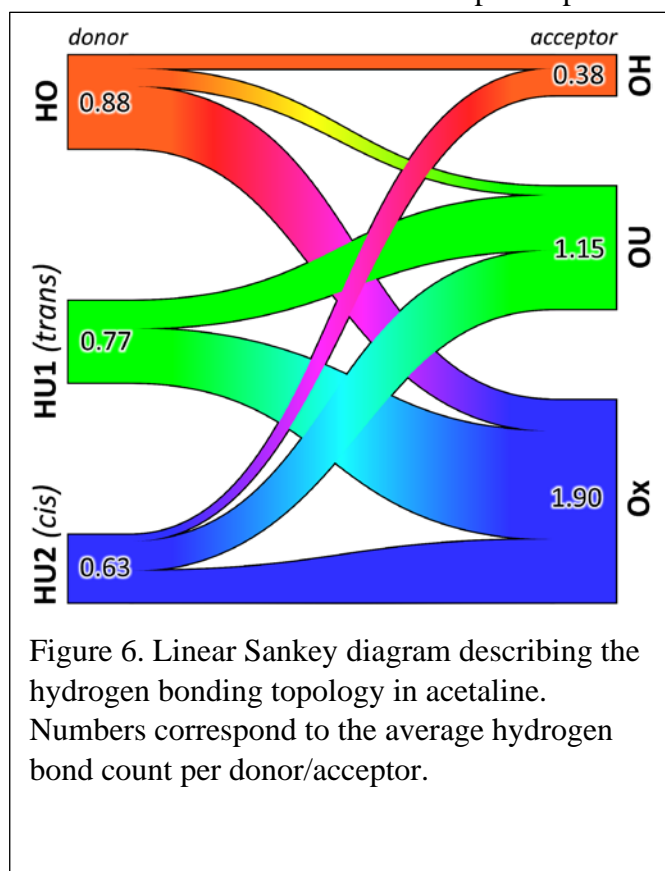


Figure 6. Linear Sankey diagram describing the hydrogen bonding topology in acetaline. Numbers correspond to the average hydrogen bond count per donor/acceptor.

the linear Sankey diagram approach of **Figure 6**, introduced recently for this kind of analysis.³⁹ A wealth of information can be straightforwardly extracted from such a plot, on the nature of HB networking in acetaline. The hydrogen bond donated by choline OH (HOH) (upper left) is mainly involved with the acetate Ox (lower right). There is only a tiny amount of hydrogen bonding interaction between HOH and choline OH and negligible interaction with urea. The trans and cis protons of urea (HU1 and HU2, respectively) behave differently. While the trans protons (HU1, middle left) do not form hydrogen bonds to choline OH, but form strong hydrogen bonds to both urea OU and acetate Ox, the cis protons (HU2, lower left) also form hydrogen

271 bonds with choline OH. Now considering the acceptors (right side), incoming hydrogen bonds at
272 choline OH almost exclusively come from the urea cis protons, HU2. The urea oxygen receives strong
273 hydrogen bonds from both cis and trans urea's protons, while it almost receives no hydrogen bonds
274 from choline HOH. A similar picture arises for acetate Ox, where the hydrogen bond received from the
275 urea trans protons is most significant. Overall, the major role played by the acetate anion in establishing
276 HB interactions is confirmed by this graph; analogously the minor role played by choline's OH
277 acceptor site is also highlighted.

278 Additional understanding of the mutual spatial distribution of the different species with respect to each
279 other can be obtained by inspecting the spatial distribution functions reported in **Figures 7**. The first of
280 such plots refers to the distribution of the three different moieties surrounding a reference urea
281 molecule. Urea is strongly correlated with acetate anions (red lobes) at spatial locations corresponding

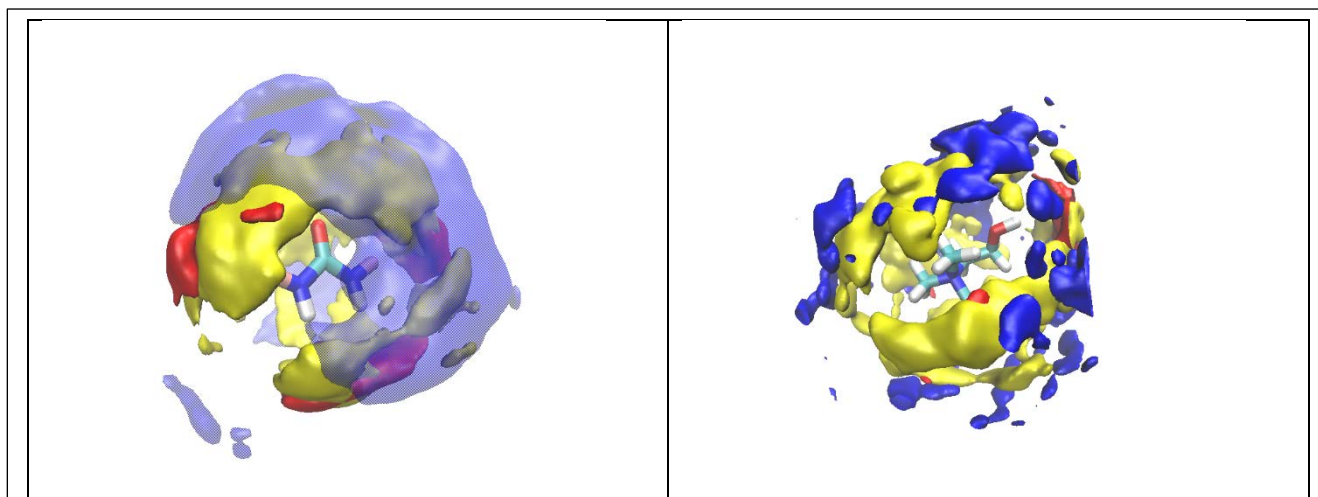


Figure 7. Spatial distribution functions around reference urea (left) and choline (right). The coloured lobes correspond to 20% most likely distribution of choline (blue), acetate (red) and urea (yellow) in acetaline

282 to its cis and trans hydrogens. Choline cations (blue lobes) distribute in a much more homogeneous
283 way around urea and correlations are not driven by HB, but rather by dispersive interactions. Finally,
284 urea (yellow lobes) competes with acetate to access the reference urea hydrogens; it moreover interacts
285 with reference urea oxygen. It also appears that choline tends to distribute around urea, aiming at
286 interacting also with the other species surrounding the reference one. In **Figure 7 b)** the distributions
287 around a reference choline cation are shown. The acetate anion is strongly interacting with the hydroxyl
288 group, with a weak competition on this site with urea; otherwise, both the choline cation and urea are

289 distributed rather homogeneously around the whole reference choline, with urea approaching closer
290 than choline the reference molecule.

291 These pictures are consistent with the overwhelming role played by acetate in HB interacting with both
292 urea's and choline' HB donor hydrogens. On the other hand, the amphiphilic nature of urea and the
293 possibility of choline to interact not only with coulombic forces, but also with dispersive ones, make
294 these two moieties able to efficiently solvate any component in acetaline. Analogously to the case of
295 reline, an intertwining of the different species occurs in delivering an intimate mixing of these
296 components at atomic level.

297 To corroborate the structural picture emerging from the combined X-ray / Reverse Monte Carlo
298 approach, variable-temperature NMR measurements were performed. As inter-species correlations
299 appear to be dominated by HB interactions, the upfield or downfield movement of the temperature-
300 dependent ^1H chemical shift was monitored to give a preliminary insight into the strength of the HB of
301 the detected proton. **Figure 8** shows the relative shifts of the ^1H NMR signals of acetaline, which are
302 defined as $\Delta\delta = \delta - \delta_0$, with δ_0 the chemical shift of a given proton in the pure DES and δ the chemical
303 shift of the same proton for increased temperature.^{49,50} The remarkable upfield shift of urea protons is
304 compatible with a weakening of the H-bond strength at the urea site with temperature,⁵¹ and points
305 towards their strong involvement in the HB network of the mixture. No relevant changes are observed
306 for the choline signals, including the N-methyl groups, which is in line with a minor role played by the

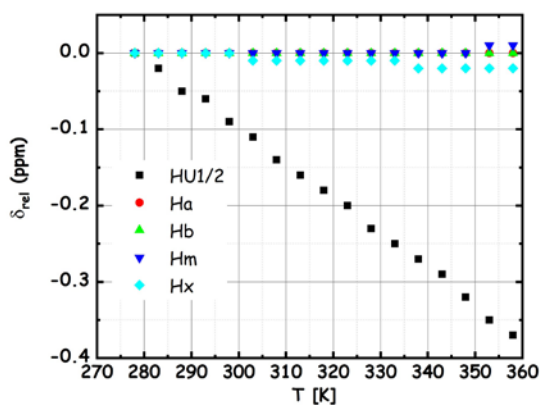


Figure 8. ^1H relative shift observed for acetaline as a function of the temperature.

cation in the intermolecular network. Only a tiny upfield shift emerges for the methyl group of acetate, as they do not directly participate in the HB interactions but most likely feel a pale indirect effect of the major role played by the acidic group of the anion.

The NMR experiments of choice to probe spatial intermolecular networks are typically based on the nuclear Overhauser enhancement (nOe). In extensively connected systems like DES it is however quite common to observe intra- and

318 inter-correlations between all sites/species in the mixtures.^{52,53} This is the case for acetaline too, as

319 displayed in **Figure S1** in the Supporting Information. **Due to spin diffusion and/or exchange**
320 **(facilitated by the residual water)**, all signals are positive. Choline shows intramolecular NOE signals,
321 and intermolecular NOE are observed between all the three species, choline, acetate and urea. As
322 expected, intense correlations are observed between the hydroxyl group proton of choline and urea, and
323 the N-methyl groups of choline and urea. The methyl group of acetate shows the strongest correlations
324 with the N-methyl protons of choline and with urea. This confirms the major role of these protons in
325 the interactions holding the DES components together.

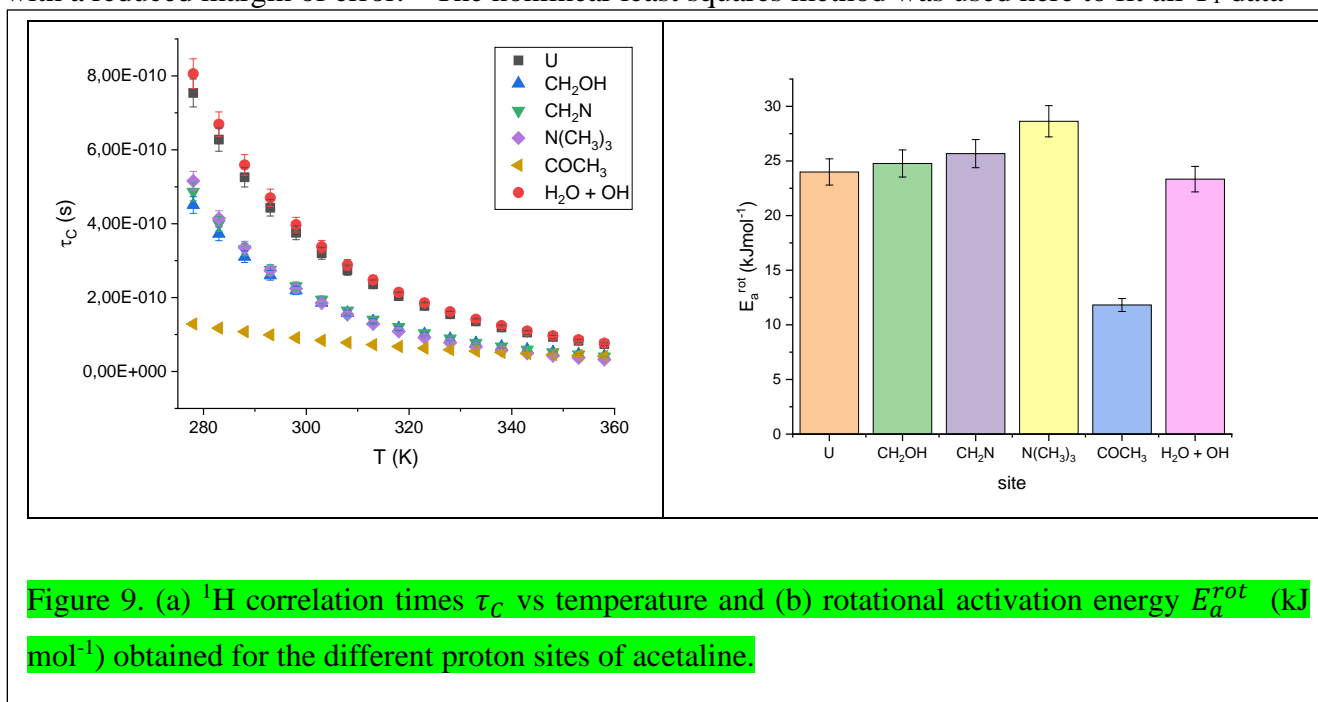
326 The NOESY data provide then support to the scenario of an extended HB network in the DES, which is
327 the root of its peculiar macroscopic properties. We also exploited relaxation and diffusion NMR
328 experiments to shed more light on the system. Intermolecular interactions and dynamics are indeed
329 intertwined, as strong correlations reduce motion – as one can intuitively envisage. T_1 relaxation times
330 and self-diffusion coefficients were measured over an 80 °C temperature interval and analyzed to get
331 quantitative descriptors of the motion(s).

332 As displayed in **Figure S2 in the Supporting Information**, all temperature-dependent T_1 curves, but that
333 corresponding to methyl protons of acetate, pass through a minimum. This indicates that the protons of
334 choline and urea undergo a transition from the extreme narrowing ($\omega_0\tau_c < 1$) to the diffusion limit
335 ($\omega_0\tau_c > 1$) relaxation regime between ~25 °C and ~50 °C. Contrarily, the methyl protons of the anion
336 fail to undergo this transition in the studied temperature range due to their higher mobility. In the case
337 of ^1H T_1 , where the predominant relaxation mechanism is the homonuclear dipole–dipole interaction,
338 the relaxation rate R_1 is defined by the Bloembergen, Purcell, and Pound (BPP) approach as:^{54–56}

$$339 \quad R_1 = \frac{1}{T_1} = C \left(\frac{\tau_c}{1 + \omega_0^2\tau_c^2} + \frac{4\tau_c}{1 + 4\omega_0^2\tau_c^2} \right) \quad (1)$$

340 with ω_0 the observe frequency (rad s^{-1}) and C a term evaluated separately for each nucleus. The
341 correlation time of the dipolar interaction τ_c can be thought of as the time required for the vector
342 connecting the interacting nuclei to rotate through the angle of one radian, and for small rigid
343 molecules it commonly reflects the molecular reorientational time constant.⁵⁶ As for flexible ionic
344 liquids^{57,58}, the τ_c observed for acetamine have to be rather considered as a combination of molecular
345 reorientation and internal motions of each given segment. From the term in brackets in Eq. (1), it
346 follows that T_1 is minimum when $\omega_0\tau_c = 2\pi\nu_0\tau_c = 0.616$ ^{58–60}, which means here $\tau_c = 0.616/(2\pi \cdot$
347 $500.13 \cdot 10^6 \text{ Hz}) = 196 \text{ ps}$. Such minimum T_1 value can be used to calculate C from Eq. (1), then

348 enabling the calculations of τ_C values from the T_1 values observed at any temperature. The
 349 temperature-dependent correlation times can be then used in an Arrhenius-type equation to calculate
 350 the “apparent” activation energy E_a^{rot} (averaged over several types of movements).^{58,61} Alternatively,
 351 by substituting the function of the correlation time approximated as an Arrhenius expression into the
 352 BPP equation (Eq. (1)), and assuming C temperature insensitive, the combined equation can be directly
 353 solved yielding the same outputs within the experimental error.^{58,62} Although the two methods are
 354 essentially the same from the theoretical standpoint, the latter nonlinear least squares method is useful
 355 in cases where an exact minimum is not reached in the examined temperature range, and is
 356 recommended even for protons where a T_1 minimum can be distinctly observed as it needs less steps
 357 with a reduced margin of error.⁵⁸ The nonlinear least squares method was used here to fit all T_1 data



358 obtaining the correlation times and activation energies reported in **Figure 9**. All temperature-dependent
 359 curves followed perfectly the BPP model, which means that a single basic motion occurs in the studied
 360 temperature range.⁵⁹ The best-fit parameters are given in **Table S1** in the Supporting Information,
 361 together with those obtained by applying the most widely used method based on the T_1 minimum
 362 followed by Arrhenius plot of the activation energies, to confirm that comparable results are obtained.
 363 Urea protons show the longest τ_C values (slowest rotational motion), and the methyl protons of acetate
 364 the shortest ones (fastest rotational motion), while the three methylene and methyl sites of choline
 365 exhibited all close, intermediate τ_C values. A direct comparison between the correlation times of the
 366 different sites and species is complicated due to the contribution of different relaxation mechanisms.

367 More informative are the rotational activation energies, which mark a significant difference between
368 acetate from the one side, with E_a^{rot} of ca. 12 kJ mol⁻¹, and choline and urea from the other, all with
369 E_a^{rot} above 20 kJ mol⁻¹. Hence, the rotational motion of the acetate protons is not only the fastest, also
370 due to the intramolecular rotation around the symmetry axis of the methyl group, but it also requires
371 less energy to occur. For the sake of completeness, we also report the correlation times and rotational
372 activation energy obtained from the BPP analysis of the temperature-dependent T₁ data of the peak
373 corresponding to the residual water and the hydroxyl proton of choline (Figures S2 and 9). All T₁, τ_C
374 and E_a^{rot} values essentially overlap those corresponding to urea protons, pointing towards a strong
375 correlation between the rotational motion of the two species. Despite its relevance, the role of water in
376 the intermolecular network of ChOAc:U is beyond the scope of the present paper and will be deepened
377 in a separate work on hydrated acetaline. Here the focus is on the role of the DES constituents -
378 choline, acetate and urea - and we can safely assume that the residual water molecules will participate
379 in the intermolecular network without drastic alterations of the mutual relationships among them.

380 In order to monitor the translational mobility and gather a more complete overview of the system, the
381 self-diffusion coefficients of the different acetaline moieties were measured by PFG NMR. The
382 diffusivities, D, probed in the range 278 – 358 K are given in Figure S3 and Table S2 in the
383 Supporting Information. As expected, the diffusion coefficients measured for the methylene protons of
384 choline yielded the same value as CH₃, hence only the latter is presented. The temperature dependence

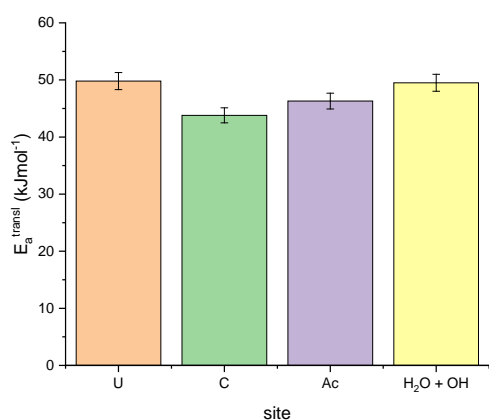


Figure 10. Translational activation energy E_a^{transl} (kJmol⁻¹) obtained for all species in acetaline.

of the diffusion coefficients over the whole probed temperature range was modelled in terms of an Arrhenius-activated process. Translational activation energies are reported in Figure 10 and fit parameters in Table S3 in the Supporting Information. While the activation energies associated with relaxation data are in the range 10–30 kJ mol⁻¹, the activation energies associated with diffusion data are larger (40–50 kJ mol⁻¹). This is due to the different molecular motion affecting these apparent activation energies, rotational *versus* translational, and is in agreement with behaviours found for instance in ionic

398 liquids.^{63,64} Noteworthy is the order of E_a^{transl} : urea \approx H₂O + OH > acetate > choline. This is unrelated
399 to the molecular size of the species and can be explained only by admitting that the translational motion
400 of urea and acetate is slowed down by their strong involvement in the HB network. The major role of
401 urea and acetate in the intermolecular network, inferred here from a dynamic parameter, fits the
402 molecular picture outlined by means of more common techniques for structure elucidation, such as X-
403 ray and NOESY. Note, also, that this prominent role is maintained here even in the presence of residual
404 amounts of water (5.7 wt%). Contrarily, the activation energy of choline is the lowest one regardless of
405 its higher size due to its less fundamental role in the intermolecular connections. As urea has proven to
406 strongly connect with other constituents in several DES using both the oxygen and proton nuclei (see
407 also the linear Sankey diagram in **Figure 6**), its reduced rotational and translational mobility (high E_a^{rot}
408 and E_a^{transl}) is quite expected. The peculiar role of acetate is instead not a foregone conclusion. The
409 key role of this small anion in the HB network keeps it on a tight leash, strongly affecting its
410 translational mobility and increasing its E_a^{transl} , which is a dynamic indicator of the whole molecule.
411 Contrarily, the rotational mobility of the methyl protons of acetate does not suffer from a strong effect,
412 as they are not directly participating in the HB network. Hence the corresponding E_a^{rot} - a local
413 dynamic parameter - is still smaller than the rotational activation energy of all other proton sites of both
414 choline and urea.

415

416

417

418 **Conclusion.**

419 Choline acetate mixtures with urea at a stoichiometric composition of 1:2, here termed as acetaline, are
420 deep eutectic media. Acetaline's melting point is ca. 40 °C, but it can be easily supercooled into the
421 liquid state at sub-ambient conditions. Liquid acetaline structure at atomistic level has been
422 investigated by means of synchrotron high energy X-ray diffraction, supported by the EPSR Reverse
423 Monte Carlo analysis approach that allows extracting detailed information on the mutual interactions
424 between acetaline's moieties. Hydrogen bonding plays a major role in determining structure in liquid
425 acetaline. Radial distribution functions shows how acetate-mediated HB are among the strongest in the
426 system; urea plays also a major role as HB donor and these correlations are straightforwardly described
427 by the use of a Sankey diagram illustrating HB flow among the different donor and acceptor moieties.
428 A complex intertwining of different moieties is observed with coulombic interactions (via HB
429 correlations) mostly involving acetate and urea, while choline is involved mostly in dispersive
430 interactions. This peculiar situation is mirrored in the dynamics monitored in acetaline. While acetate's
431 methyl group shows the lowest correlation times and activation energy considering ¹H rotational
432 motion, the anion diffuses slower than expected from its size, thus confirming its strong role in the HB
433 network. Choline turns out to be the moiety with the lowest activation energy concerning diffusive
434 dynamics, reflecting its secondary involvement into the HB interactions network.

435 **Acknowledgements.**

436 This work has been supported by the University of Rome Sapienza Projects: "Microscopic and
437 mesoscopic organization in ionic liquid-based systems." (RG11715C7CC660BE) and "Green solvents
438 for simple and complex carbohydrates" (RM120172B2165468).

439 M.B. acknowledges financial support by the Deutsche Forschungsgemeinschaft (DFG) through project
440 Br 5494/1-1.

441 M.E.D.P. thanks Politecnico di Milano for her postdoctoral fellowship in the framework of the "MSCA
442 EF Master Class 2018" funding programme.

443 Access to Prof. S. Brutti's laboratories (Univ. Rome – Sapienza) is gratefully acknowledged.

444 We thank Diamond Light Source for access to beamline I15-1 (CY27222-1) that contributed to the
445 results presented here.

446

447

448

449 **DATA AVAILABILITY.**

450

451 The data that support the findings of this study are available from the corresponding authors upon
452 reasonable request.

453

454

455 **References**

- 456 (1) Abbott, A. P.; Capper, G.; Davies, D. L.; Rasheed, R. K.; Tambyrajah, V. Novel Solvent
457 Properties of Choline Chloride/Urea Mixtures. *Chem. Commun.* **2003**, No. 1, 70–71.
458 <https://doi.org/10.1039/b210714g>.
- 459 (2) Abbott, A. P.; Boothby, D.; Capper, G.; Davies, D. L.; Rasheed, R. K. Deep Eutectic Solvents
460 Formed between Choline Chloride and Carboxylic Acids: Versatile Alternatives to Ionic
461 Liquids. *J. Am. Chem. Soc.* **2004**, *126* (29), 9142–9147. <https://doi.org/10.1021/ja048266j>.
- 462 (3) Smith, E. L.; Abbott, A. P.; Ryder, K. S. Deep Eutectic Solvents (DESs) and Their Applications.
463 *Chem. Rev.* **2014**, *114* (21), 11060–11082. <https://doi.org/10.1021/cr300162p>.
- 464 (4) Wagle, D. V.; Zhao, H.; Baker, G. A. Deep Eutectic Solvents: Sustainable Media for Nanoscale
465 and Functional Materials. *Acc. Chem. Res.* **2014**, *47* (8), 2299–2308.
466 <https://doi.org/10.1021/ar5000488>.
- 467 (5) Zhang, Q.; De Oliveira Vigier, K.; Royer, S.; Jérôme, F. Deep Eutectic Solvents: Syntheses,
468 Properties and Applications. *Chem. Soc. Rev.* **2012**, *41* (21), 7108–7146.
469 <https://doi.org/10.1039/c2cs35178a>.
- 470 (6) Paiva, A.; Craveiro, R.; Aroso, I.; Martins, M.; Reis, R. L.; Duarte, A. R. C. Natural Deep
471 Eutectic Solvents - Solvents for the 21st Century. *ACS Sustain. Chem. Eng.* **2014**, *2* (5), 1063–
472 1071. <https://doi.org/10.1021/sc500096j>.
- 473 (7) Roda, A.; Matias, A.; Paiva, A.; Duarte, A. Polymer Science and Engineering Using Deep
474 Eutectic Solvents. *Polymers (Basel)*. **2019**, *11* (5), 912. <https://doi.org/10.3390/polym11050912>.
- 475 (8) Perna, F. M.; Vitale, P.; Capriati, V. Deep Eutectic Solvents and Their Applications as Green
476 Solvents. *Curr. Opin. Green Sustain. Chem.* **2020**, *21*, 27–33.
477 <https://doi.org/10.1016/j.cogsc.2019.09.004>.
- 478 (9) Perkins, S. L.; Painter, P.; Colina, C. M. Molecular Dynamic Simulations and Vibrational
479 Analysis of an Ionic Liquid Analogue. *J. Phys. Chem. B* **2013**, *117* (35), 10250–10260.
480 <https://doi.org/10.1021/jp404619x>.
- 481 (10) Hammond, O. S.; Bowron, D. T.; Edler, K. J. Liquid Structure of the Choline Chloride-Urea

- 482 Deep Eutectic Solvent (Reline) from Neutron Diffraction and Atomistic Modelling. *Green*
483 *Chem.* **2016**, *18* (9), 2736–2744. <https://doi.org/10.1039/c5gc02914g>.
- 484 (11) Gilmore, M.; Moura, L. M.; Turner, A. H.; Swadźba-Kwaśny, M.; Callear, S. K.; McCune, J. A.;
485 Scherman, O. A.; Holbrey, J. D. A Comparison of Choline:Urea and Choline:Oxalic Acid Deep
486 Eutectic Solvents at 338 K. *J. Chem. Phys.* **2018**, *148* (19). <https://doi.org/10.1063/1.5010246>.
- 487 (12) Fetisov, E. O.; Harwood, D. B.; Kuo, I. F. W.; Warrag, S. E. E.; Kroon, M. C.; Peters, C. J.;
488 Siepmann, J. I. First-Principles Molecular Dynamics Study of a Deep Eutectic Solvent: Choline
489 Chloride/Urea and Its Mixture with Water. *J. Phys. Chem. B* **2018**, *122* (3), 1245–1254.
490 <https://doi.org/10.1021/acs.jpcc.7b10422>.
- 491 (13) Kaur, S.; Sharma, S.; Kashyap, H. K.; Kaur, S.; Sharma, S.; Kashyap, H. K. Bulk and Interfacial
492 Structures of Reline Deep Eutectic Solvent : A Molecular Dynamics Study Bulk and Interfacial
493 Structures of Reline Deep Eutectic Solvent : A Molecular Dynamics Study. *J. Chem. Phys.* **2017**,
494 *147*, 194507. <https://doi.org/10.1063/1.4996644>.
- 495 (14) Ashworth, C. R.; Matthews, R. P.; Welton, T.; Hunt, P. A. Doubly Ionic Hydrogen Bond
496 Interactions within the Choline Chloride-Urea Deep Eutectic Solvent. *Phys. Chem. Chem. Phys.*
497 **2016**, *18* (27), 18145–18160. <https://doi.org/10.1039/c6cp02815b>.
- 498 (15) Triolo, A.; Lo Celso, F.; Russina, O. Structural Features of β -Cyclodextrin Solvation in the Deep
499 Eutectic Solvent, Reline. *J. Phys. Chem. B* **2020**, *124* (13), 2652–2660.
500 <https://doi.org/10.1021/acs.jpcc.0c00876>.
- 501 (16) Di Pietro, M. E.; Hammond, O.; van den Bruinhorst, A.; Mannu, A.; Padua, A.; Mele, A.; Costa
502 Gomes, M. Connecting Chloride Solvation with Hydration in Deep Eutectic Systems. *Phys.*
503 *Chem. Chem. Phys.* **2021**, *23* (1), 107–111. <https://doi.org/10.1039/D0CP05843B>.
- 504 (17) Gilmore, M.; Swadzba-Kwasny, M.; Holbrey, J. D. Thermal Properties of Choline
505 Chloride/Urea System Studied under Moisture-Free Atmosphere. *J. Chem. Eng. Data* **2019**, *64*
506 (12), 5248–5255. <https://doi.org/10.1021/acs.jced.9b00474>.
- 507 (18) Gabriele, F.; Chiarini, M.; Germani, R.; Tiecco, M.; Spreti, N. Effect of Water Addition on
508 Choline Chloride/Glycol Deep Eutectic Solvents: Characterization of Their Structural and
509 Physicochemical Properties. *J. Mol. Liq.* **2019**, *291*, 111301.

- 510 <https://doi.org/10.1016/j.molliq.2019.111301>.
- 511 (19) Wagle, D. V.; Baker, G. A.; Mamontov, E. Differential Microscopic Mobility of Components
512 within a Deep Eutectic Solvent. *J. Phys. Chem. Lett.* **2015**, *6* (15), 2924–2928.
513 <https://doi.org/10.1021/acs.jpcllett.5b01192>.
- 514 (20) Stefanovic, R.; Ludwig, M.; Webber, G. B.; Atkin, R.; Page, A. J. Nanostructure, Hydrogen
515 Bonding and Rheology in Choline Chloride Deep Eutectic Solvents as a Function of the
516 Hydrogen Bond Donor. *Phys. Chem. Chem. Phys.* **2017**, *19* (4), 3297–3306.
517 <https://doi.org/10.1039/c6cp07932f>.
- 518 (21) Turner, A. H.; Holbrey, J. D. Investigation of Glycerol Hydrogen-Bonding Networks in Choline
519 Chloride/Glycerol Eutectic-Forming Liquids Using Neutron Diffraction. *Phys. Chem. Chem.*
520 *Phys.* **2019**, *21* (39), 21782–21789. <https://doi.org/10.1039/c9cp04343h>.
- 521 (22) Perkins, S. L.; Painter, P.; Colina, C. M. Experimental and Computational Studies of Choline
522 Chloride-Based Deep Eutectic Solvents. *J. Chem. Eng. Data* **2014**, *59* (11), 3652–3662.
523 <https://doi.org/10.1021/je500520h>.
- 524 (23) Kaur, S.; Malik, A.; Kashyap, H. K. Anatomy of Microscopic Structure of Ethaline Deep
525 Eutectic Solvent Decoded through Molecular Dynamics Simulations. *J. Phys. Chem. B* **2019**,
526 *123* (39), 8291–8299. <https://doi.org/10.1021/acs.jpccb.9b06624>.
- 527 (24) Zhang, Y.; Poe, D.; Heroux, L.; Squire, H.; Doherty, B. W.; Long, Z.; Dadmun, M.; Gurkan, B.;
528 Tuckerman, M. E.; Maginn, E. J. Liquid Structure and Transport Properties of the Deep Eutectic
529 Solvent Ethaline. *J. Phys. Chem. B* **2020**, *124* (25), 5251–5264.
530 <https://doi.org/10.1021/acs.jpccb.0c04058>.
- 531 (25) Zhang, H.; Ferrer, M. L.; Roldán-Ruiz, M. J.; Jiménez-Riobóo, R. J.; Gutiérrez, M. C.; Del
532 Monte, F. Brillouin Spectroscopy as a Suitable Technique for the Determination of the Eutectic
533 Composition in Mixtures of Choline Chloride and Water. *J. Phys. Chem. B* **2020**, *124* (19),
534 4002–4009. <https://doi.org/10.1021/acs.jpccb.0c01919>.
- 535 (26) Rahman, M. S.; Raynie, D. E. Thermal Behavior, Solvatochromic Parameters, and Metal Halide
536 Solvation of the Novel Water-Based Deep Eutectic Solvents. *J. Mol. Liq.* **2020**, *3*, 114779.
537 <https://doi.org/10.1016/j.molliq.2020.114779>.

- 538 (27) Triolo, A.; Lo Celso, F.; Brehm, M.; Di Lisio, V.; Russina, O. Liquid Structure of a Choline
539 Chloride-Water Natural Deep Eutectic Solvent: A Molecular Dynamics Characterization. *J. Mol.*
540 *Liq.* **2021**, *331*, 115750. <https://doi.org/10.1016/j.molliq.2021.115750>.
- 541 (28) Fukaya, Y.; Iizuka, Y.; Sekikawa, K.; Ohno, H. Bio Ionic Liquids: Room Temperature Ionic
542 Liquids Composed Wholly of Biomaterials. *Green Chem.* **2007**, *9* (11), 1155–1157.
543 <https://doi.org/10.1039/b706571j>.
- 544 (29) Zhao, H.; Baker, G. A.; Holmes, S. New Eutectic Ionic Liquids for Lipase Activation and
545 Enzymatic Preparation of Biodiesel. *Org. Biomol. Chem.* **2011**, *9* (6), 1908–1916.
546 <https://doi.org/10.1039/c0ob01011a>.
- 547 (30) Hoppe, J.; Drozd, R.; Byzia, E.; Smiglak, M. Deep Eutectic Solvents Based on Choline Cation -
548 Physicochemical Properties and Influence on Enzymatic Reaction with β -Galactosidase. *Int. J.*
549 *Biol. Macromol.* **2019**, *136*, 296–304. <https://doi.org/10.1016/j.ijbiomac.2019.06.027>.
- 550 (31) Colombo Dugoni, G.; Mezzetta, A.; Guazzelli, L.; Chiappe, C.; Ferro, M.; Mele, A. Purification
551 of Kraft Cellulose under Mild Conditions Using Choline Acetate Based Deep Eutectic Solvents.
552 *Green Chem.* **2020**, 8680–8691. <https://doi.org/10.1039/d0gc03375h>.
- 553 (32) Filik, J.; Ashton, A. W.; Chang, P. C. Y.; Chater, P. A.; Day, S. J.; Drakopoulos, M.; Gerring,
554 M. W.; Hart, M. L.; Magdysyuk, O. V.; Michalik, S.; Smith, A.; Tang, C. C.; Terrill, N. J.;
555 Wharmby, M. T.; Wilhelm, H. Processing Two-Dimensional X-Ray Diffraction and Small-
556 Angle Scattering Data in DAWN 2. *J. Appl. Crystallogr.* **2017**, *50* (3), 959–966.
557 <https://doi.org/10.1107/S1600576717004708>.
- 558 (33) Soper, A. K.; Barney, E. R. Extracting the Pair Distribution Function from White-Beam X-Ray
559 Total Scattering Data. *J. Appl. Crystallogr.* **2011**, *44* (4), 714–726.
560 <https://doi.org/10.1107/S0021889811021455>.
- 561 (34) Soper, A. K. The Radial Distribution Functions of Water as Derived from Radiation Total
562 Scattering Experiments: Is There Anything We Can Say for Sure? *ISRN Phys. Chem.* **2013**,
563 *2013*, 1–67. <https://doi.org/10.1155/2013/279463>.
- 564 (35) Soper, A. K. Empirical Potential Monte Carlo Simulation of Fluid Structure. *Chem. Phys.* **1996**,
565 *202* (2–3), 295–306. [https://doi.org/10.1016/0301-0104\(95\)00357-6](https://doi.org/10.1016/0301-0104(95)00357-6).

- 566 (36) Soper, A. K.; Castner, E. W.; Luzar, A. Impact of Urea on Water Structure: A Clue to Its
567 Properties as a Denaturant? *Biophys. Chem.* **2003**, *105* (2–3), 649–666.
568 [https://doi.org/10.1016/S0301-4622\(03\)00095-4](https://doi.org/10.1016/S0301-4622(03)00095-4).
- 569 (37) Bowron, D. T.; D’Agostino, C.; Gladden, L. F.; Hardacre, C.; Holbrey, J. D.; Lagunas, M. C.;
570 McGregor, J.; Mantle, M. D.; Mullan, C. L.; Youngs, T. G. A. Structure and Dynamics of 1-
571 Ethyl-3-Methylimidazolium Acetate via Molecular Dynamics and Neutron Diffraction. *J. Phys.*
572 *Chem. B* **2010**, *114* (23), 7760–7768. <https://doi.org/10.1021/jp102180q>.
- 573 (38) Brehm, M.; Kirchner, B. TRAVIS - A Free Analyzer and Visualizer for Monte Carlo and
574 Molecular Dynamics Trajectories. *J. Chem. Inf. Model.* **2011**, *51* (8), 2007–2023.
575 <https://doi.org/10.1021/ci200217w>.
- 576 (39) Brehm, M.; Thomas, M.; Gehrke, S.; Kirchner, B. TRAVIS—A Free Analyzer for Trajectories
577 from Molecular Simulation. *J. Chem. Phys.* **2020**, *152* (16), 164105.
578 <https://doi.org/10.1063/5.0005078>.
- 579 (40) Hollőczki, O.; Macchiagodena, M.; Weber, H.; Thomas, M.; Brehm, M.; Stark, A.; Russina, O.;
580 Triolo, A.; Kirchner, B. Triphasic Ionic-Liquid Mixtures: Fluorinated and Non-Fluorinated
581 Aprotic Ionic-Liquid Mixtures. *ChemPhysChem* **2015**, *16* (15), 3325–3333.
582 <https://doi.org/10.1002/cphc.201500473>.
- 583 (41) McDonald, S.; Murphy, T.; Imberti, S.; Warr, G. G.; Atkin, R. Amphiphilically Nanostructured
584 Deep Eutectic Solvents. *J. Phys. Chem. Lett.* **2018**, *9* (14), 3922–3927.
585 <https://doi.org/10.1021/acs.jpcllett.8b01720>.
- 586 (42) Triolo, A.; Russina, O.; Bleif, H. J.; Di Cola, E. Nanoscale Segregation in Room Temperature
587 Ionic Liquids. *J. Phys. Chem. B* **2007**, *111* (18), 4641–4644. <https://doi.org/10.1021/jp067705t>.
- 588 (43) Russina, O.; Triolo, A.; Gontrani, L.; Caminiti, R. Mesoscopic Structural Heterogeneities in
589 Room-Temperature Ionic Liquids. *J. Phys. Chem. Lett.* **2012**, *3* (1), 27–33.
590 <https://doi.org/10.1021/jz201349z>.
- 591 (44) Macchiagodena, M.; Ramondo, F.; Triolo, A.; Gontrani, L.; Caminiti, R. Liquid Structure of 1-
592 Ethyl-3-Methylimidazolium Alkyl Sulfates by x-Ray Scattering and Molecular Dynamics. *J.*
593 *Phys. Chem. B* **2012**, *116* (45), 13448–13458. <https://doi.org/10.1021/jp306982e>.

- 594 (45) Russina, O.; Sferrazza, A.; Caminiti, R.; Triolo, A. Amphiphile Meets Amphiphile: Beyond the
595 Polar-Apolar Dualism in Ionic Liquid/Alcohol Mixtures. *J. Phys. Chem. Lett.* **2014**, *5* (10),
596 1738–1742. <https://doi.org/10.1021/jz500743v>.
- 597 (46) Schroer, W.; Triolo, A.; Russina, O. Nature of Mesoscopic Organization in Protic Ionic Liquid-
598 Alcohol Mixtures. *J. Phys. Chem. B* **2016**, *120* (9), 2638–2643.
599 <https://doi.org/10.1021/acs.jpcc.6b01422>.
- 600 (47) Russina, O.; Lo Celso, F.; Plechkova, N. V.; Triolo, A. Emerging Evidences of Mesoscopic-
601 Scale Complexity in Neat Ionic Liquids and Their Mixtures. *J. Phys. Chem. Lett.* **2017**, *8* (6),
602 1197–1204. <https://doi.org/10.1021/acs.jpcclett.6b02811>.
- 603 (48) Hammond, O. S.; Bowron, D. T.; Jackson, A. J.; Arnold, T.; Sanchez-Fernandez, A.;
604 Tsapatsaris, N.; Garcia Sakai, V.; Edler, K. J. Resilience of Malic Acid Natural Deep Eutectic
605 Solvent Nanostructure to Solidification and Hydration. *J. Phys. Chem. B* **2017**, *121* (31), 7473–
606 7483. <https://doi.org/10.1021/acs.jpcc.7b05454>.
- 607 (49) Posada, E.; Roldán-Ruiz, M. J.; Jiménez Riobóo, R. J.; Gutiérrez, M. C.; Ferrer, M. L.; del
608 Monte, F. Nanophase Separation in Aqueous Dilutions of a Ternary DES as Revealed by
609 Brillouin and NMR Spectroscopy. *J. Mol. Liq.* **2019**, *276*, 196–203.
610 <https://doi.org/10.1016/j.molliq.2018.11.139>.
- 611 (50) Hall, C. A.; Le, K. A.; Rudaz, C.; Radhi, A.; Lovell, C. S.; Damion, R. A.; Budtova, T.; Ries, M.
612 E. Macroscopic and Microscopic Study of 1-Ethyl-3-Methyl-Imidazolium Acetate-Water
613 Mixtures. *J. Phys. Chem. B* **2012**, *116* (42), 12810–12818. <https://doi.org/10.1021/jp306829c>.
- 614 (51) Grzesiek, S.; Becker, E. D. Hydrogen Bonding. In *Encyclopedia of Magnetic Resonance*; John
615 Wiley & Sons, Ltd: Chichester, UK, 2011.
616 <https://doi.org/10.1002/9780470034590.emrstm0216.pub2>.
- 617 (52) Häkkinen, R.; Alshammari, O.; Timmermann, V.; D'Agostino, C.; Abbott, A. Nanoscale
618 Clustering of Alcoholic Solutes in Deep Eutectic Solvents Studied by Nuclear Magnetic
619 Resonance and Dynamic Light Scattering. *ACS Sustain. Chem. Eng.* **2019**, *7* (17), 15086–15092.
620 <https://doi.org/10.1021/acssuschemeng.9b03771>.
- 621 (53) Delso, I.; Lafuente, C.; Muñoz-Embido, J.; Artal, M. NMR Study of Choline Chloride-Based

- 622 Deep Eutectic Solvents. *J. Mol. Liq.* **2019**, *290*. <https://doi.org/10.1016/j.molliq.2019.111236>.
- 623 (54) Bloembergen, N.; Purcell, E. M.; Pound, R. V. Relaxation Effects in Nuclear Magnetic
624 Resonance Absorption. *Phys. Rev.* **1948**, *73* (7), 679–712.
625 <https://doi.org/10.1103/PhysRev.73.679>.
- 626 (55) Hayamizu, K.; Tsuzuki, S.; Seki, S.; Umebayashi, Y. Nuclear Magnetic Resonance Studies on
627 the Rotational and Translational Motions of Ionic Liquids Composed of 1-Ethyl-3-
628 Methylimidazolium Cation and Bis(Trifluoromethanesulfonyl)Amide and
629 Bis(Fluorosulfonyl)Amide Anions and Their Binary Systems Including Lithium Salts. *J. Chem.*
630 *Phys.* **2011**, *135* (8). <https://doi.org/10.1063/1.3625923>.
- 631 (56) Hayamizu, K.; Tsuzuki, S.; Seki, S.; Umebayashi, Y. Multinuclear NMR Studies on
632 Translational and Rotational Motion for Two Ionic Liquids Composed of BF₄ Anion. *J. Phys.*
633 *Chem. B* **2012**, *116* (36), 11284–11291. <https://doi.org/10.1021/jp306146s>.
- 634 (57) Alam, T. M.; Dreyer, D. R.; Bielwaski, C. W.; Ruoff, R. S. Measuring Molecular Dynamics and
635 Activation Energies for Quaternary Acyclic Ammonium and Cyclic Pyrrolidinium Ionic Liquids
636 Using ¹⁴N NMR Spectroscopy. *J. Phys. Chem. A* **2011**, *115* (17), 4307–4316.
637 <https://doi.org/10.1021/jp200630k>.
- 638 (58) Di Pietro, M. E.; Castiglione, F.; Mele, A. Polar/Apolar Domains' Dynamics in
639 Alkylimidazolium Ionic Liquids Unveiled by the Dual Receiver NMR ¹H and ¹⁹F Relaxation
640 Experiment. *J. Mol. Liq.* **2021**, *322*, 114567. <https://doi.org/10.1016/j.molliq.2020.114567>.
- 641 (59) Bystrov, S. S.; Matveev, V. V.; Chernyshev, Y. S.; Balevičius, V.; Chizhik, V. I. Molecular
642 Mobility in a Set of Imidazolium-Based Ionic Liquids [Bmim]⁺A⁻ by the NMR-Relaxation
643 Method. *J. Phys. Chem. B* **2019**, *123* (10), 2362–2372. <https://doi.org/10.1021/acs.jpccb.8b11250>.
- 644 (60) Shimizu, Y.; Wachi, Y.; Fujii, K.; Imanari, M.; Nishikawa, K. NMR Study on Ion Dynamics and
645 Phase Behavior of a Piperidinium-Based Room-Temperature Ionic Liquid: 1-Butyl-1-
646 Methylpiperidinium Bis(Fluorosulfonyl)Amide. *J. Phys. Chem. B* **2016**, *120* (25), 5710–5719.
647 <https://doi.org/10.1021/acs.jpccb.6b04095>.
- 648 (61) Antony, J. H.; Mertens, D.; Dölle, A.; Wasserscheid, P.; Carper, W. R. Molecular
649 Reorientational Dynamics of the Neat Ionic Liquid 1-Butyl-3-Methylimidazolium

- 650 Hexafluorophosphate by Measurement of ^{13}C Nuclear Magnetic Relaxation Data.
651 *ChemPhysChem* **2003**, *4* (6), 588–594. <https://doi.org/10.1002/cphc.200200603>.
- 652 (62) Bayley, P. M.; Best, A. S.; MacFarlane, D. R.; Forsyth, M. The Effect of Coordinating and Non-
653 Coordinating Additives on the Transport Properties in Ionic Liquid Electrolytes for Lithium
654 Batteries. *Phys. Chem. Chem. Phys.* **2011**, *13* (10), 4632–4640.
655 <https://doi.org/10.1039/c0cp02084b>.
- 656 (63) Hayamizu, K.; Tsuzuki, S.; Seki, S.; Fujii, K.; Suenaga, M.; Umebayashi, Y. Studies on the
657 Translational and Rotational Motions of Ionic Liquids Composed of N-Methyl-N-Propyl-
658 Pyrrolidinium (P13) Cation and Bis(Trifluoromethanesulfonyl)Amide and
659 Bis(Fluorosulfonyl)Amide Anions and Their Binary Systems Including Lithium Salts. *J. Chem.*
660 *Phys.* **2010**, *133* (19), 194505. <https://doi.org/10.1063/1.3505307>.
- 661 (64) Di Pietro, M. E.; Castiglione, F.; Mele, A. Anions as Dynamic Probes for Ionic Liquid Mixtures.
662 *J. Phys. Chem. B* **2020**, *124* (14), 2879–2891. <https://doi.org/10.1021/acs.jpcc.0c00026>.
- 663
664
665